

Computed tomography (CT)

Jiří Hozman, Jan Kybic

2005–2019

Základní uspořádání systému CT



CT history

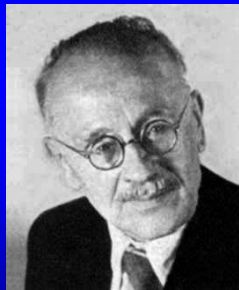
- 1917** mathematical theory (Radon)
- 1956** tomography reconstruction in radioastronomy (Bracewell)
- 1963** CT reconstruction theory
- 1971** CT principles demonstrated (Hounsfield)
- 1972** first working CT for humans (EMI, London, Hounsfield)
- 1973** PET
- 1974** Ultrasound tomography
- 1982** SPECT
- 1985** Helical CT
- 1998** Multislice CT, 0.5 s/frame

Johann Radon

(matematik)

* 16.12.1887 Děčín, ČR

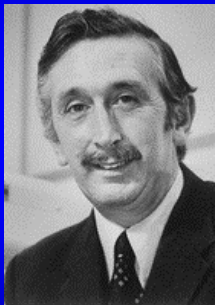
† 25.5.1956 Vídeň, Rakousko



1917 - "Über die Bestimmung von
Funktionen durch ihre Integral-werte
langs gewisser Mannigfaltigkeiten",
*Berichte Sachsische Akademie der
Wissenschaften. Leipzig, Math.-Phis. Kl.,*
v.69, pp. 262-267. V této práci pan Radon
matematicky vyřešil rekonstrukci
prostorového obrazu na základě znalosti
jeho projekcí.

Sir Godfrey Newbold Hounsfield

1919-2004



Nottinghamshire, samouk, nenavštěvoval univerzitu
Nobelova cena 1979

Sir Godfrey Hounsfield
Nobel Prize in Medicine, 1979

[2]



Gamma Ray Source: 28,000
measurements, 9 day collection,
2.5 hour recon, 2hour display.

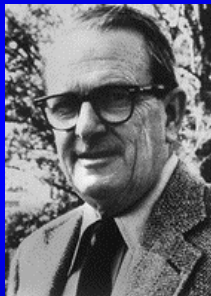
X-ray source reduced collection
to 9 hours. Clinical model
took 18 sec

[1]



EMI-1, 1971:
Atkinson Morley Hospital, England

Allan M. Cormack



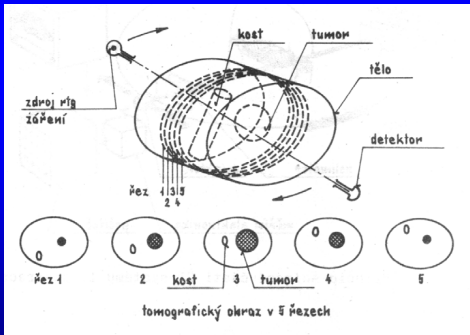
1924-1998, narozen v Johannesburgu

Tomography modalities

- ▶ x-rays — CT
- ▶ gamma rays — PET, SPECT
- ▶ light — optical tomography
- ▶ RF waves — MRI
- ▶ DC — electric impedance tomography
- ▶ ultrasound — ultrasound tomography

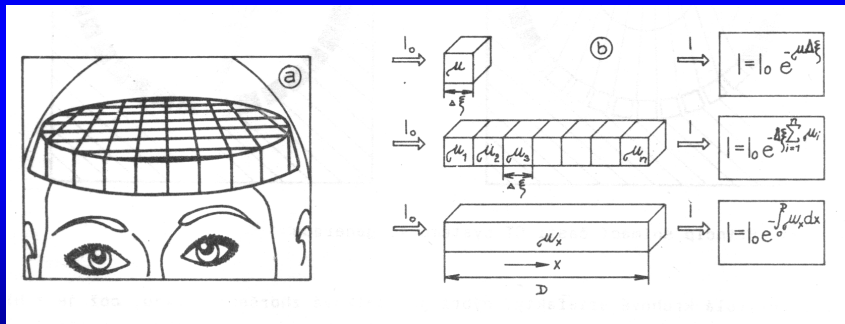
Základní princip CT

CT vytváří obraz těla pacienta jako sérii tomografických sekcí (řezů). Každý řez je vytvořen matematickou rekonstrukcí předmětu ze znalosti průmětů (projekcí) předmětu do různých směrů.

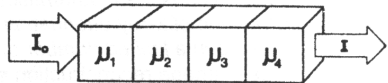
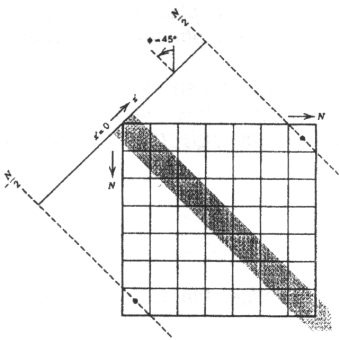


Základní princip CT

Jednotlivé řezy objektu musí být rozděleny do sítě malých objemových elementů (voxels) se čtvercovou základnou a s konstantní hodnotou útlumu.

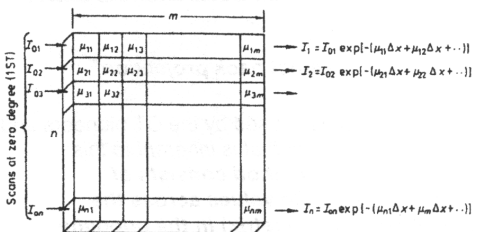


Základní fyzikální princip CT

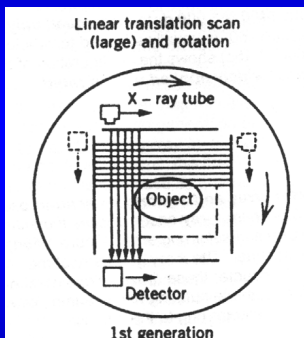
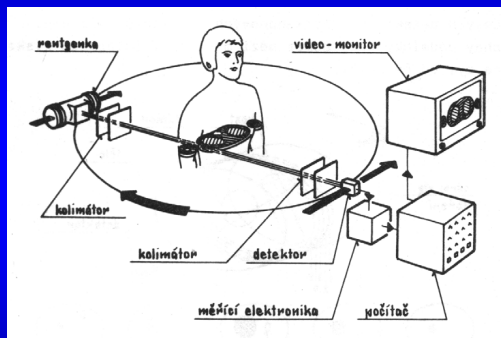


$$I = I_0 e^{-(\mu_1 + \mu_2 + \mu_3 + \mu_4) x}$$

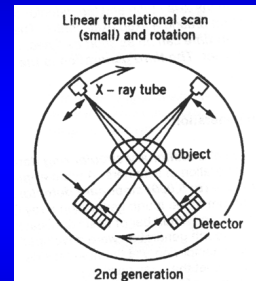
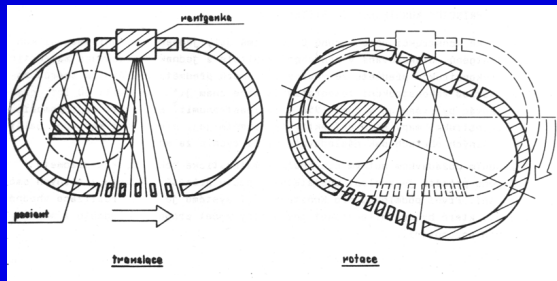
(a)



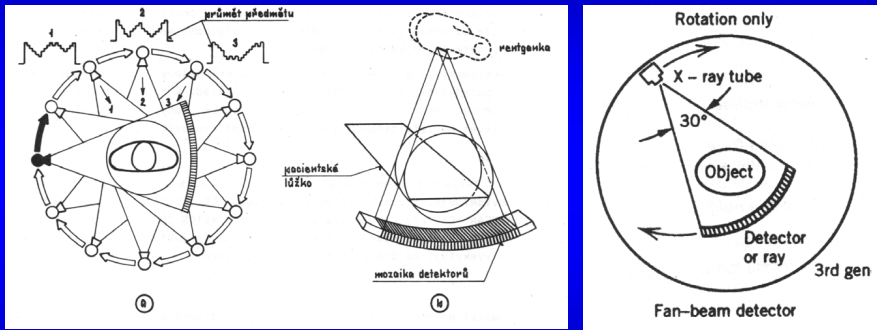
CT systémy 1. generace



CT systémy 2. generace

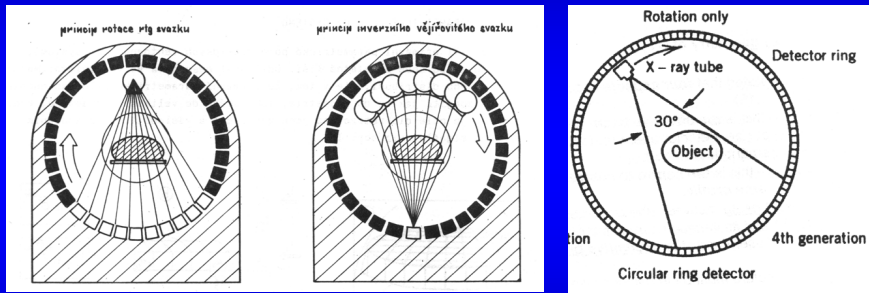


CT systémy 3. generace



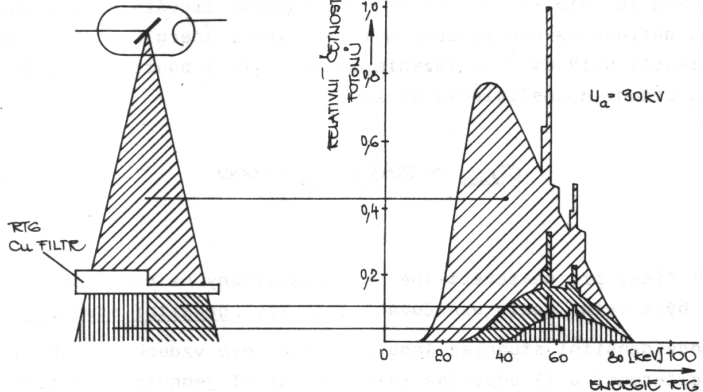
asi nejčastěji používané

CT systémy 4. generace

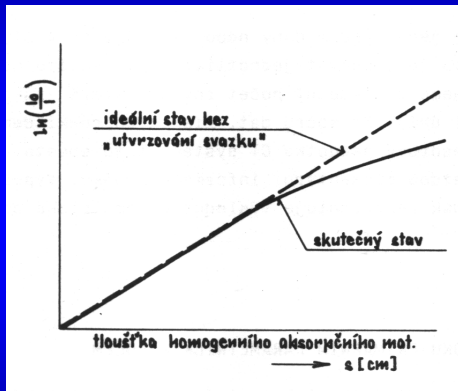


Rotuje jen zdroj, detektory stabilní

„Utvrzování svazku“ (beam hardening)



„Utvrzování svazku“ (beam hardening)



CT číslo - Haunsfieldovo číslo (HU)

Je vyjádřením kvantitativního hodnocení absorbčních vlastností tkáně.

$$CT = K \cdot \frac{\text{tkáně} - \text{vody}}{\text{vody}}$$

$K = 1000$
 $\text{vody} = 0,19 \text{ cm}^{-1}$

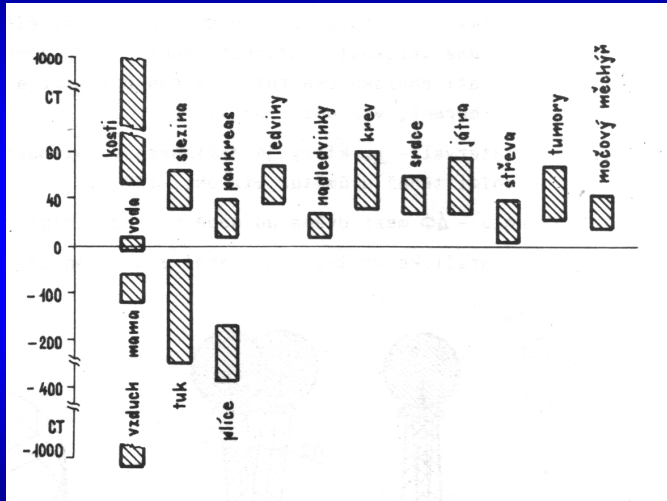
Měřeno monochromatickým zářením 73 keV.

$$CT = 5263 \cdot \text{tkáně} - 1000$$

stupnice CT čísel = denzitní stupnice

rozsah od -1000 až zhruba +1000, pro vzduch -1000,
pro vodu 0

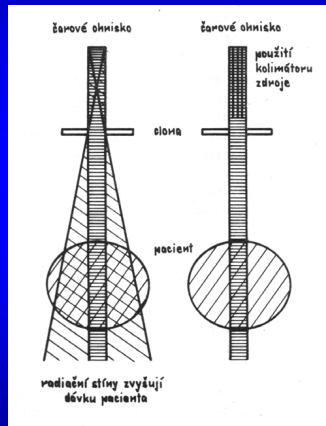
CT číslo - Haunsfieldovo číslo (HU)



Generace, zpracování a detekce radiačního signálu CT systémů

CT systémy 2. generace (několik detektorů)

- pomalé a rychlé systémy
- sendvičový a lamelový kolimátor



Generace, zpracování a detekce radiačního signálu CT systémů

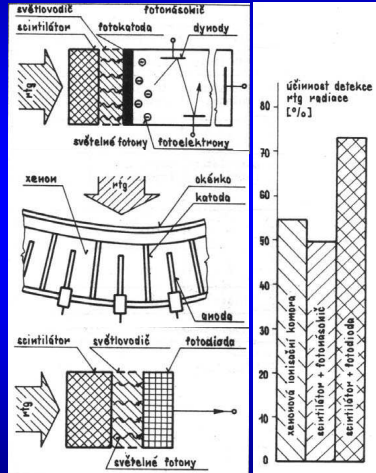
Detektory

scintilační detektor (krystal)
+ fotonásobič

ionizační komory plněné
plynem (xenon)

scintilační detektor (krystal)
+ fotodioda (fototranzistor)

Flat-panel detector (FPD)
Thin-film transistor (TFT) array



Základní principy rekonstrukce obrazu

$\sigma(\xi, \eta)$ denzitní funkce =
předmětová funkce

lin. součinitel

zeslabení

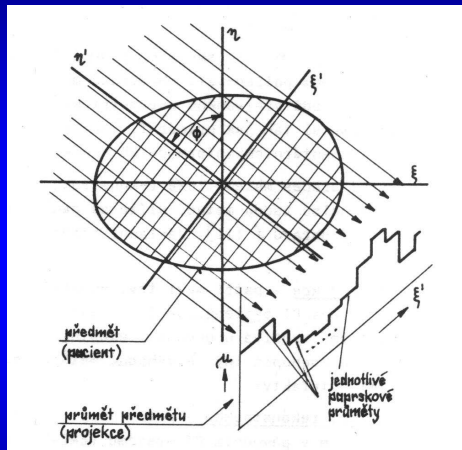
(ξ, η) původní souř.

Φ snímací úhel

ξ' rotovaná souř.

η' rotovaná souř.

$p(\xi', \Phi)$ paprskový součet či průmět



Základní principy rekonstrukce obrazu

$$p(\xi', \Phi) = \int o(\xi, \eta) d\eta \quad I = I_0 \exp \left[- \int o(\xi, \eta) d\eta \right]$$

$$o(\xi, \eta) \approx \boxed{o(\xi', \eta)}$$

$$\boxed{p(\xi', \Phi) = - \ln \frac{I_0}{I}}$$

$$\boxed{\xi' = \xi \cdot \cos \Phi + \eta \cdot \sin \Phi}$$

$$\xi = \xi' \cdot \cos \Phi - \eta \cdot \sin \Phi$$

$$\eta' = -\xi \cdot \sin \Phi + \eta \cdot \cos \Phi$$

$$\eta = \xi' \cdot \sin \Phi + \eta \cdot \cos \Phi$$

Radon transform

Projection in polar coordinates:

$$P_\varphi(\xi') = \mathcal{R}[o(\xi, \eta)]$$

$$P_\varphi(\xi') = \int_L o(\xi, \eta) d\ell$$

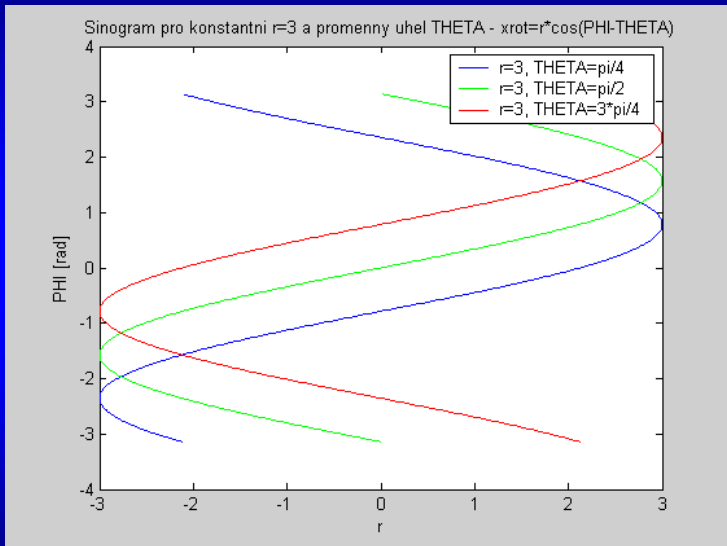
along the line L defined by φ a ξ' :

$$\xi' = \xi \cos \varphi + \eta \sin \varphi$$

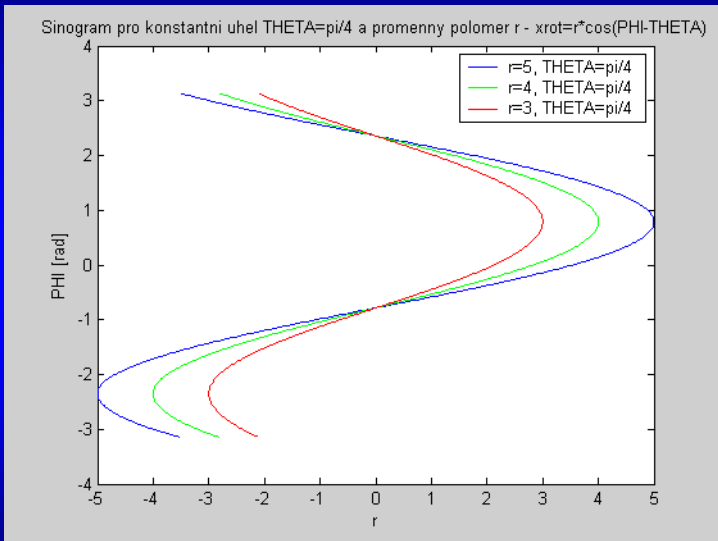
Equivalently

$$P_\varphi(\xi') = \int o(\xi' \cos \varphi - \eta' \sin \varphi, \xi' \sin \varphi + \eta' \cos \varphi) d\eta'$$

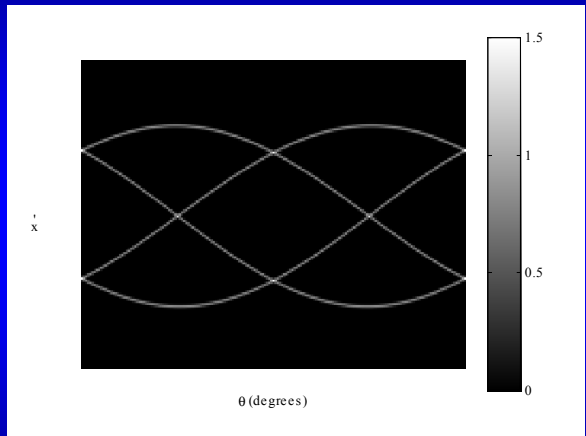
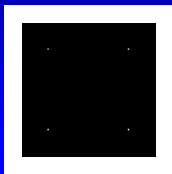
Radonova transformace



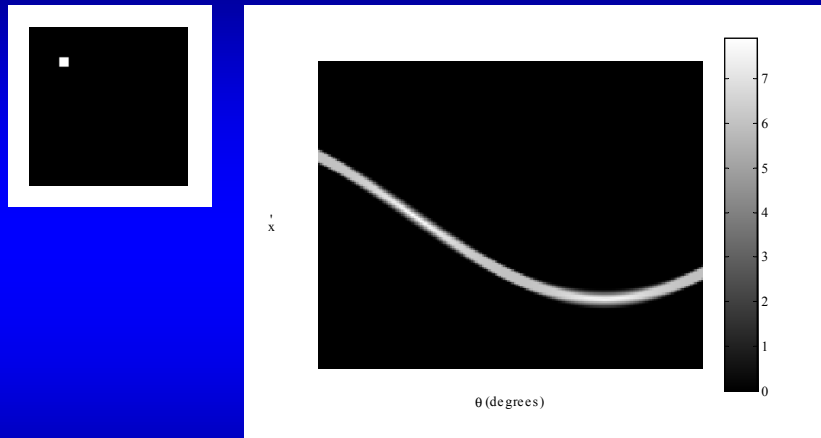
Radonova transformace



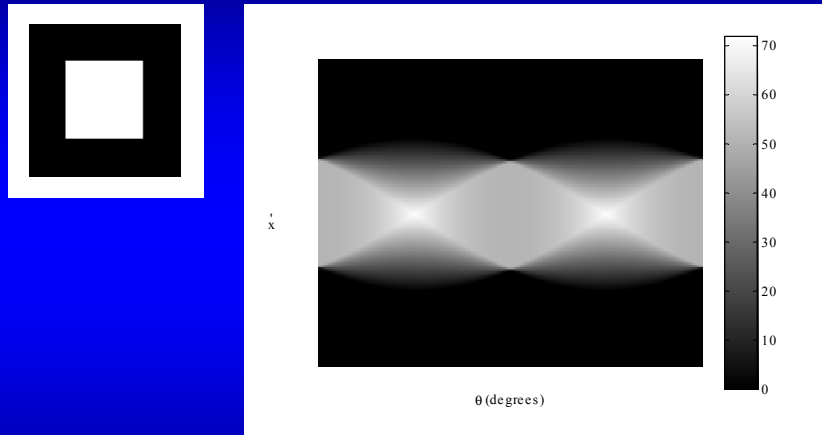
Radonova transformace



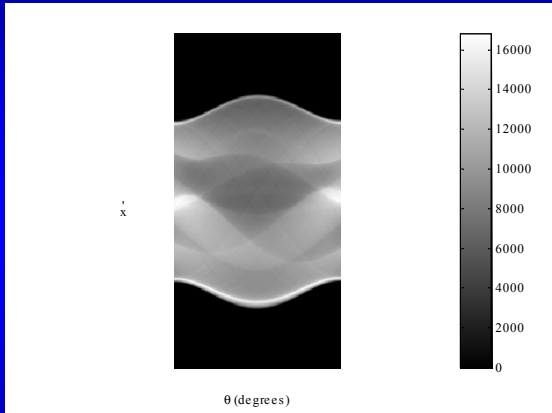
Radonova transformace



Radonova transformace

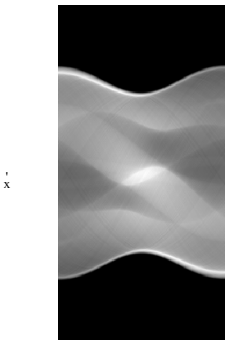


Radonova transformace

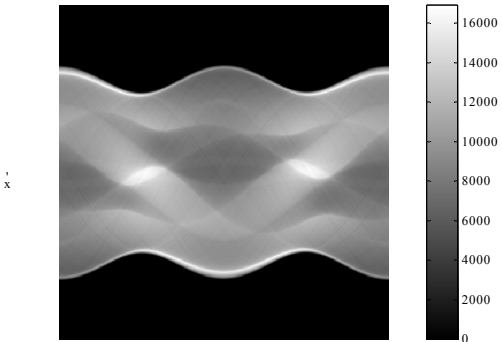


Shepp-Logan fantom

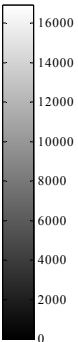
Radonova transformace



θ (degrees)



θ (degrees)



Periodicity RT vůči úhlu

Reconstruction methods

- ▶ *Backprojection*
- ▶ *Fourier reconstruction*
- ▶ Filtered backprojection
- ▶ Algebraic reconstruction (iterative)

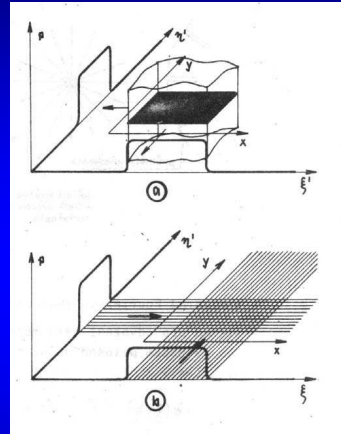
Přímá zpětná projekce

$$i(x,y) = \sum_{j=1}^m p(\xi_j, \Phi_j) \Delta \Phi$$

Φ_j j-tý projekční úhel

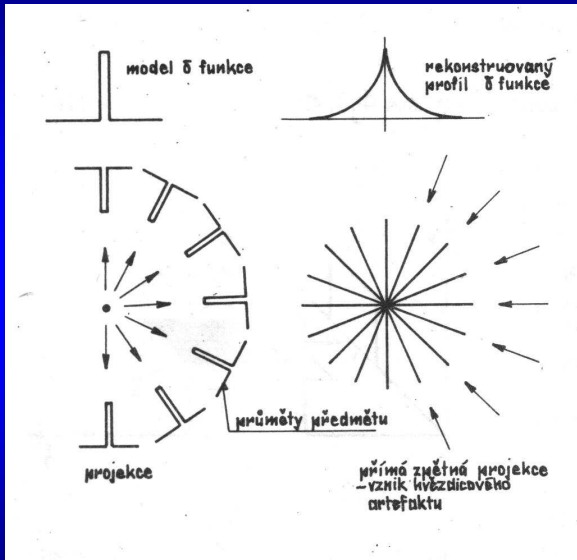
$\Delta \Phi$ úhlový přírůstek
mezi projekcemi

m počet projekcí



$$i(x,y) = \sum_{j=1}^m p((x \cdot \cos \Phi_j + y \cdot \sin \Phi_j), \Phi_j) \Delta \Phi$$

Přímá zpětná projekce - hvězdicový artefakt



Central slice theorem

Projection Theorem, Věta o centrálním řezu)

$$P_\varphi(\xi') = \int o(\xi' \cos \varphi - \eta' \sin \varphi, \xi' \sin \varphi + \eta' \cos \varphi) d\eta'$$

Fourier transform of the Radon transform by ξ' :

$$\begin{aligned}\mathcal{F} \{ \mathcal{R}[o(\xi, \eta)] \} &= \mathcal{F} \{ P_\varphi(\xi') \} = \hat{P}_\varphi(\omega) = \int P_\varphi(\xi') e^{-2\pi j \omega \xi'} d\xi' \\ &= \iint o(\xi' \cos \varphi - \eta' \sin \varphi, \xi' \sin \varphi + \eta' \cos \varphi) e^{-2\pi j \omega \xi'} d\xi' d\eta'\end{aligned}$$

Substitution $(\xi', \eta') \rightarrow (\xi, \eta)$:

$$\hat{P}_\varphi(\omega) = \int o(\xi, \eta) e^{-2\pi j \omega (\xi \cos \varphi + \eta \sin \varphi)} d\xi d\eta$$

Central slice theorem

$$\hat{P}_\varphi(\omega) = \int o(\xi, \eta) e^{-2\pi j \omega (\xi \cos \varphi + \eta \sin \varphi)} d\xi d\eta$$

Denote $u = \omega \cos \varphi$ $v = \omega \sin \varphi$

$$\hat{P}(u, v) = \int o(\xi, \eta) e^{-2\pi j (\xi u + \eta v)} d\xi d\eta$$

and therefore

$$\hat{P}(u, v) = \mathcal{F}\{o(\xi, \eta)\}$$

$$\hat{P}_\varphi(\omega) = \mathcal{F}\{o(\xi, \eta)\}(\omega \cos \varphi, \omega \sin \varphi) = \hat{o}(\omega \cos \varphi, \omega \sin \varphi)$$

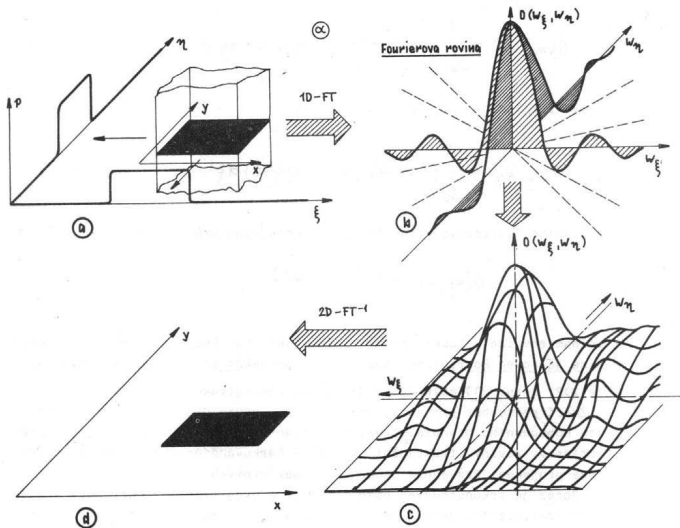
Central slice theorem

$$\hat{P}(u, v) = \mathcal{F}\{o(\xi, \eta)\}$$

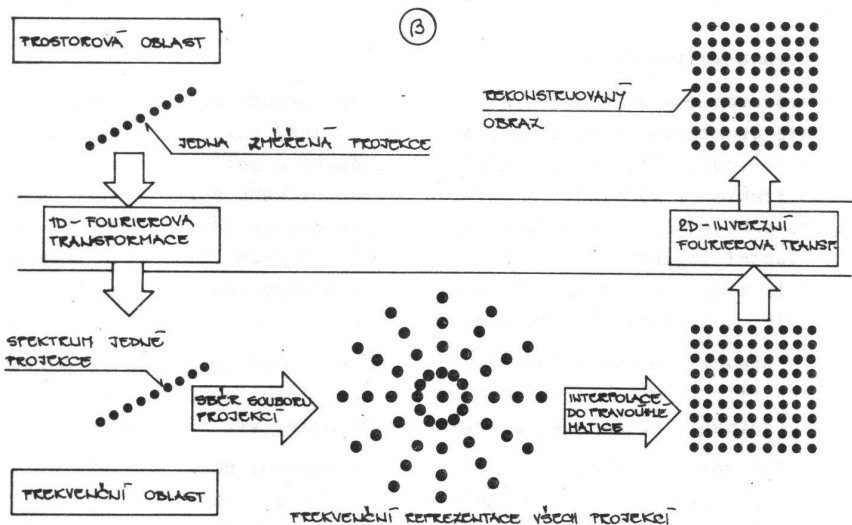
$$\hat{P}_\varphi(\omega) = \mathcal{F}\{o(\xi, \eta)\}(\omega \cos \varphi, \omega \sin \varphi) = \hat{o}(\omega \cos \varphi, \omega \sin \varphi)$$

Slice of the 2D Fourier transform of the image o at angle φ is the 1D Fourier transform of the projection P_φ of the same image o .

Analytická rekonstrukce - 2D FT



Analytická rekonstrukce - 2D FT



Inverse Radonova transform

From the Fourier slice theorem:

$$\hat{P}(u, v) = \mathcal{F} \{o(\xi, \eta)\}$$

$$o(\xi, \eta) = \mathcal{F}^{-1} \left\{ \hat{P}(u, v) \right\} = \int_{-\infty}^{\infty} \int_{-\infty}^{\infty} \hat{P}(u, v) e^{2\pi j(\xi u + \eta v)} du dv$$

Polar coordinates $u = \omega \cos \varphi$, $v = \omega \sin \varphi$:

$$o(\xi, \eta) = \int_0^{\pi} \int_{-\infty}^{\infty} \hat{P}_{\varphi}(\omega) e^{2\pi j\omega(\xi \cos \varphi + \eta \sin \varphi)} |\omega| d\omega d\varphi$$

where $|\omega|$ is the Jacobian (determinant).

Inverse Radonova transform

$$o(\xi, \eta) = \int_0^{\pi} \int_{-\infty}^{\infty} \hat{P}_{\varphi}(\omega) e^{2\pi j \omega (\xi \cos \varphi + \eta \sin \varphi)} |\omega| d\omega d\varphi$$

can be written as

$$o(\xi, \eta) = \int_0^{\pi} Q_{\varphi}(\underbrace{\xi \cos \varphi + \eta \sin \varphi}_{\xi'}) d\varphi$$

$$Q_{\varphi}(\xi') = \int_{-\infty}^{\infty} \hat{P}_{\varphi}(\omega) e^{2\pi j \omega \xi'} |\omega| d\omega$$

where $Q_{\varphi}(\xi')$ is a modified projection

Inverse Radonova transform

$$o(\xi, \eta) = \int_0^\pi Q_\varphi(\xi') d\varphi$$

$$Q_\varphi(\xi') = \int_{-\infty}^{\infty} \hat{P}_\varphi(\omega) e^{2\pi j \omega \xi'} |\omega| d\omega$$

$$Q_\varphi(\xi') = \mathcal{F}^{-1} \left\{ |\omega| \hat{P}_\varphi(\omega) \right\} = \mathcal{F}^{-1} \{ |\omega| \} * P_\varphi(\xi')$$

defining the exact inverse Radon transform

$$P_\varphi(\xi') = \mathcal{R}[o(\xi, \eta)]$$

$$o(\xi, \eta) = \mathcal{R}^{-1}[P_\varphi(\xi')]$$

Filtered backprojection

Filtrovaná zpětná projekce

- ▶ Filter all projections $P_\varphi(\xi')$ for all φ , get modified projections $Q_\varphi(\xi')$
- ▶ Backprojected modified projections and sum

$$o(\xi, \eta) = \int_0^{\pi} Q_\varphi(\xi') d\varphi$$

$$Q_\varphi(\xi') = h(t) * P_\varphi(\xi') = \mathcal{F}^{-1}\{H(\omega)\} * P_\varphi(\xi')$$

$$H(\omega) = |\omega|$$

Practical implementation of filtered backprojection

- ▶ **Problem:** Ideal filter $H(\omega) = |\omega|$ amplifies noise

- ▶ **Solution 1:** Make $\hat{P}_\varphi(\omega)$ frequency limited.

Ramakrishnan-Lakshminarayanan → Ram-Lak filter:

$$H(\omega) = \begin{cases} |\omega| & \text{if } |\omega| \leq \Omega \\ 0 & \text{otherwise} \end{cases}$$

Practical implementation of filtered backprojection

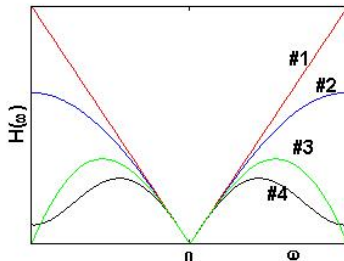
- ▶ **Problem:** Ideal filter $H(\omega) = |\omega|$ amplifies noise

- ▶ **Solution 1:** Make $\hat{P}_\varphi(\omega)$ frequency limited.

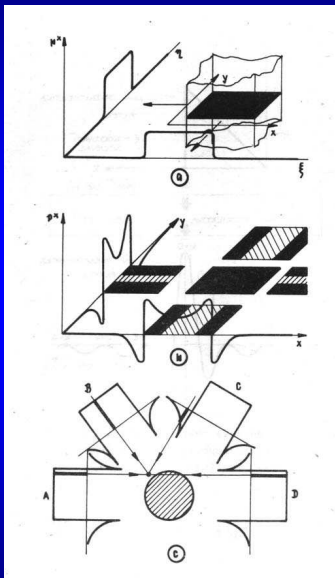
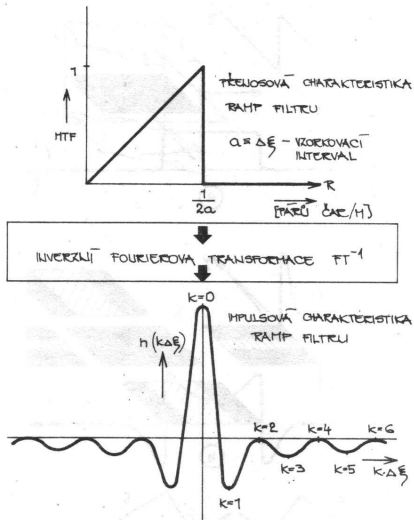
Ramakrishnan-Lakshminarayanan → Ram-Lak filter:

$$H(\omega) = \begin{cases} |\omega| & \text{if } |\omega| \leq \Omega \\ 0 & \text{otherwise} \end{cases}$$

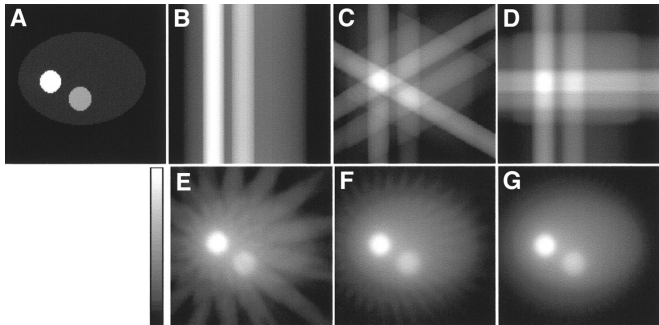
- ▶ Ram-Lak filter causes artefacts (Gibbs). Many solutions (Hamming filter, Shepp-Logan filter). Typically Hamming has better SNR but lower resolution.



Analytická rekonstrukce - filtrovaná ZP



Filtered backprojection



original image, 1,3, 4, 16, 32, a 64 projections

Algebraic rekonstruktion

- ▶ setup equations, often linear

$$p_i = \sum_j w_{ij} f_j$$

where f_j are pixel values, p_i are projections

- ▶ We know p_i and w_{ij} , solve for f_j
- ▶ Many unknowns, iterative method
 - ▶ Compare measured projections and simulations
 - ▶ Correct pixel values to decrease the difference
 - ▶ Iterate until convergence

Algebraic rekonstruktion — advantages over FBP

- ▶ Better modeling of the physics — attenuation, resolution, noise
- ▶ Better handling of limited acquisition — restricted region, restricted angles
- ▶ Can use an image model
- ▶ Less apparent artifacts

Iterativní rekonstrukce - ART

ART – Algebraic Reconstruction Technique je jedním z mnoha použitých algoritmů, které se používají do současnosti. Existují dva základní typy ART:

- aditivní

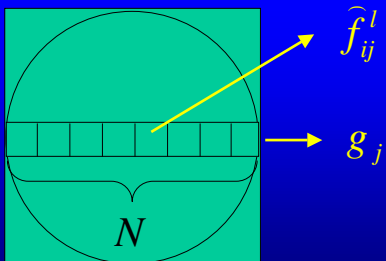
$$\hat{f}_{ij}^l = \hat{f}_{ij}^{l-1} + \frac{g_j - \sum_{i=1}^N \hat{f}_{ij}^{l-1}}{N}$$

- multiplikativní

$$\hat{f}_{ij}^l = \frac{g_j}{\sum_{i=1}^N \hat{f}_{ij}^{l-1}} \hat{f}_{ij}^{l-1}$$

Iterativní rekonstrukce – ART pokračování

- kde:
- \hat{f}_{ij}^l - odhad hodnoty i -tého voxelu podél j -tého paprsku během l -té iterace,
 - g_j - skutečný paprskový součet (data) podél j -tého paprsku,
 - N - počet objemových elementů (voxelů) podél j -tého paprsku,



Iterativní rekonstrukce – ART aditivní - příklad

- skutečná naměřená data (projekce a paprskové součty)

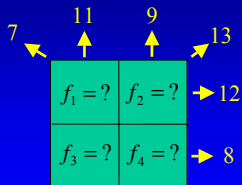
$f_1 = 5$	$f_2 = 7$	$\rightarrow 12$
$f_3 = 6$	$f_4 = 2$	$\rightarrow 8$

Diagram illustrating the iterative reconstruction process using the Additive ART (ART) method. The matrix consists of two columns of variables (f_1, f_2 and f_3, f_4) and their corresponding projections (12 and 8). The measured data values are 7 , 11 , 9 , and 13 . Arrows indicate the projection of each column onto the measured data values.

Iterativní rekonstrukce – ART př. – pokrač.

1/3
vertikální paprsky

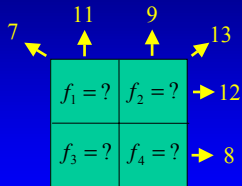
0	0
0	0



$$\hat{f}_1^{1/3} = \hat{f}_3^{1/3} = 0 + \frac{11 - 0}{2} = 5,5$$

$$\hat{f}_2^{1/3} = \hat{f}_4^{1/3} = 0 + \frac{9 - 0}{2} = 4,5$$

Iterativní rekonstrukce – ART př. – pokrač.



$$\hat{f}_1^{2/3} = 5,5 + \frac{12 - 10}{2} = 6,5$$

$$\hat{f}_2^{2/3} = 4,5 + \frac{12 - 10}{2} = 5,5$$

2/3
horizontální paprsky

5,5	4,5	$\rightarrow 10$
5,5	4,5	$\rightarrow 10$

$$\hat{f}_3^{2/3} = 5,5 + \frac{8 - 10}{2} = 4,5$$

$$\hat{f}_4^{2/3} = 4,5 + \frac{8 - 10}{2} = 3,5$$

Iterativní rekonstrukce – ART př. – pokrač.

7	11	9	13
$f_1 = ?$	$f_2 = ?$	$\rightarrow 12$	
$f_3 = ?$	$f_4 = ?$	$\rightarrow 8$	

$3/3=1$

diagonální paprsky

10	6,5	5,5	10
	4,5	3,5	

$$\hat{f}_1^1 = 6,5 + \frac{7-10}{2} = 5$$

$$\hat{f}_2^1 = 5,5 + \frac{13-10}{2} = 7$$

$$\hat{f}_3^1 = 4,5 + \frac{13-10}{2} = 6$$

$$\hat{f}_4^1 = 3,5 + \frac{7-10}{2} = 2$$

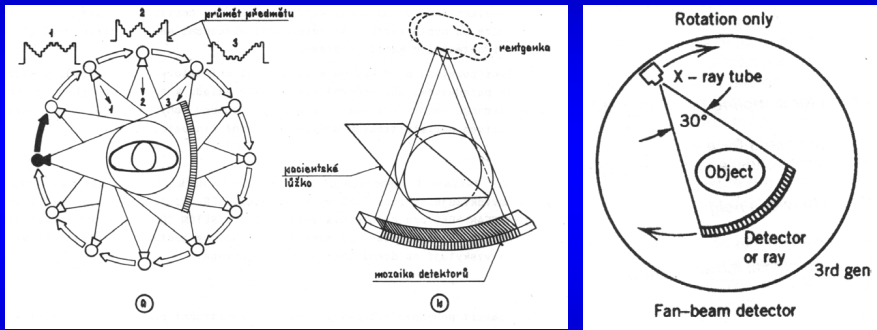
Konvergance

viz
orig.
data

Electric processing — corrections

- ▶ Offset correction (zero signal at rest)
- ▶ Normalization correction (x-ray source intensity fluctuation)
- ▶ Sensitivity correction (inhomogeneous detectors and amplifiers)
- ▶ Geometric correction
- ▶ Beam hardening correction
- ▶ Cosine correction

CT systémy 3. generace



asi nejčastěji používané

Fan-beam reconstruction

- ▶ Rays not parallel, not a Radon transform.
- ▶ Rebinning

Fan-beam reconstruction

- ▶ Rays not parallel, not a Radon transform.
- ▶ Rebinning
- ▶ Modified filtered backprojection (quadratic cosine correction, $\cos \theta$).

Fan-beam reconstruction

- ▶ Rays not parallel, not a Radon transform.
- ▶ Rebinning
- ▶ Modified filtered backprojection (quadratic cosine correction, $\cos \theta$).
- ▶ Algebraic reconstruction. Best quality but slow.

3D computed tomography

- ▶ Technical challenges: power, cooling
- ▶ Rotation method (slice by slice)
- ▶ Spiral/helix method

Spiral method

- ▶ Acceleration: 10 min → 1 min

Spiral method

- ▶ Acceleration: 10 min → 1 min
- ▶ *Pitch*:

$$P = \Delta l / d$$

Δl bed shift per rotation, d slice thickness.

Normally $0 < P < 2$. Overlap for $P < 1$. Typically $P = 1.5$.

Spiral method

- ▶ Acceleration: 10 min → 1 min
- ▶ *Pitch*:

$$P = \Delta l / d$$

Δl bed shift per rotation, d slice thickness.

Normally $0 < P < 2$. Overlap for $P < 1$. Typically $P = 1.5$.

- ▶ Interpolation in z axis

Spiral method

- ▶ Acceleration: 10 min → 1 min
- ▶ *Pitch*:

$$P = \Delta l / d$$

Δl bed shift per rotation, d slice thickness.

Normally $0 < P < 2$. Overlap for $P < 1$. Typically $P = 1.5$.

- ▶ Interpolation in z axis
- ▶ Interpolation *wide* — 1 turn. Less noise, larger effective slice thickness.

Spiral method

- ▶ Acceleration: 10 min → 1 min
- ▶ *Pitch*:

$$P = \Delta l / d$$

Δl bed shift per rotation, d slice thickness.

Normally $0 < P < 2$. Overlap for $P < 1$. Typically $P = 1.5$.

- ▶ Interpolation in z axis
- ▶ Interpolation *wide* — 1 turn. Less noise, larger effective slice thickness.
- ▶ Interpolation *Slim* — 1/2 turn, symmetry. More noise, smaller effective slice thickness.

Spiral method

- ▶ Acceleration: 10 min → 1 min
- ▶ *Pitch*:

$$P = \Delta l / d$$

Δl bed shift per rotation, d slice thickness.

Normally $0 < P < 2$. Overlap for $P < 1$. Typically $P = 1.5$.

- ▶ Interpolation in z axis
- ▶ Interpolation *wide* — 1 turn. Less noise, larger effective slice thickness.
- ▶ Interpolation *Slim* — 1/2 turn, symmetry. More noise, smaller effective slice thickness.
- ▶ Multislice acquisition — acceleration.

Radiation dose

- ▶ Absorbed dose D . 1 Gy (gray) = 1 J/kg Before 1 Gy = 100 rad
- ▶ Effective dose equivalent (dávkový ekvivalent)
 H_E [Sv] (sievert)

$$H_E = \sum_i w_i H_i$$

$H = cD$. Quality factor c is 1 for X-rays and γ rays, 10 for neutrons, 20 for α particles.

Coefficient w is organ dependent: male/female glands 0.2, lungs 0.12, breast 0.1, stomach 0.12, thyroid gland 0.05, skin 0.01.

Before 1 Sv = 100 rem

Radiation dose

- ▶ Absorbed dose D . 1 Gy (gray) = 1 J/kg Before 1 Gy = 100 rad
- ▶ Effective dose equivalent (dávkový ekvivalent)
 H_E [Sv] (sievert)

$$H_E = \sum_i w_i H_i$$

$H = cD$. Quality factor c is 1 for X-rays and γ rays, 10 for neutrons, 20 for α particles.

Coefficient w is organ dependent: male/female glands 0.2, lungs 0.12, breast 0.1, stomach 0.12, thyroid gland 0.05, skin 0.01.

Before 1 Sv = 100 rem

- ▶ Sum the doses

Radiation dose

- ▶ Medical limit (USA) is 50 mSv/year (=limit for a person working with radiation in CR), corresponding to 1000 chest X-rays, or 15 head CTs, or 5 whole body CTs (1 CT \approx 10 mSv).
- ▶ low-dose CT \approx 2 ~ 5 mSv, PET \approx 25 mSv
- ▶ In CR radioactive background about 3 mSv/year (mainly radon), similar to USA. In Colorado (altitude 1500 ~ 4000 m) about 4.5 mSv/year. Mean dose from medical imaging 0.3 mSv/year, about 3 long flights.

Radiation dose

- ▶ Medical limit (USA) is 50 mSv/year (=limit for a person working with radiation in CR), corresponding to 1000 chest X-rays, or 15 head CTs, or 5 whole body CTs (1 CT \approx 10 mSv).
- ▶ low-dose CT \approx 2 ~ 5 mSv, PET \approx 25 mSv
- ▶ In CR radioactive background about 3 mSv/year (mainly radon), similar to USA. In Colorado (altitude 1500 ~ 4000 m) about 4.5 mSv/year. Mean dose from medical imaging 0.3 mSv/year, about 3 long flights.
- ▶ cancer related death 20 %. 1 CT=10 mSv — relative increase by $10^{-3} \sim 10^{-4}$

CT image quality

- ▶ Parameters:
 - ▶ Resolution (0.5 mm)
 - ▶ Contrast (δH , about 5 – 10 H.j.)
 - ▶ Detection threshold (about 1 mm at $\Delta H = 200$, 5 mm at $\Delta H = 5$).
 - ▶ Noise (SNR)
- ▶ Artifacts
 - ▶ Scanner defects, malfunctions, operator error
 - ▶ Metal parts (shadows)
 - ▶ Motion artifacts
 - ▶ Partial volume

Artifact examples

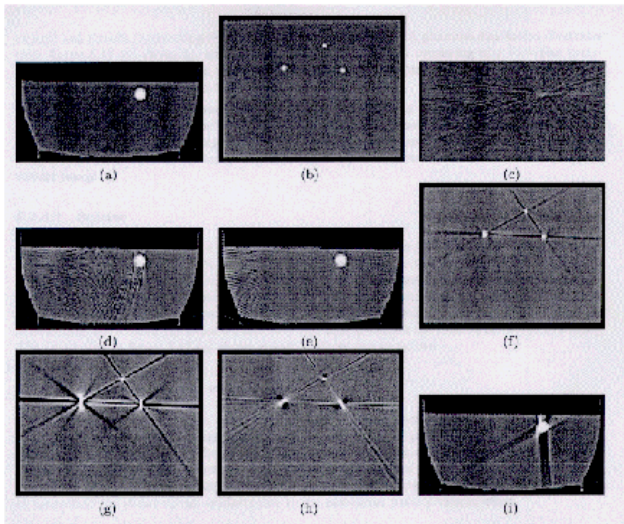


Figure 2.19 Example of image artifacts: (a) test phantom, (b) second phantom, (c) noise, (d) detector under-sampling, (e) view under-sampling, (f) beam hardening, (g) scatter, (h) nonlinear partial volume effect, and (i) object motion. (unpublished results)

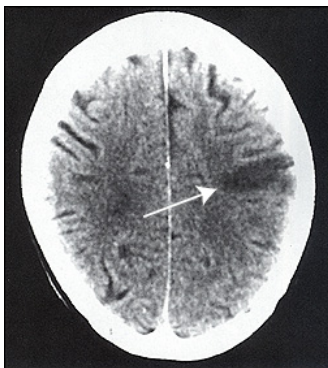
Clinical applications

- ▶ Lungs



Clinical applications

- ▶ Lungs
- ▶ Head



Clinical applications

- ▶ Lungs
- ▶ Head
- ▶ Abdomen



Computed tomography, conclusions

- ▶ Excellent spatial resolution
- ▶ 3D image
- ▶ Fast acquisition
- ▶ Weak soft tissue contrast
- ▶ Reconstruction algorithm
- ▶ Radiation dose